

## Ion-assisted nucleation and growth of GaN on sapphire(0001)

R. L. Headrick and S. Kycia

*Cornell High Energy Synchrotron Source, Cornell University, Ithaca, New York 14853*

A. R. Woll and J. D. Brock

*School of Applied and Engineering Physics, Cornell University, Ithaca, New York 14853*

M. V. Ramana Murty

*Laboratory of Atomic and Solid State Physics, Cornell University, Ithaca, New York 14853*

(Received 19 February 1998)

We have performed a real-time x-ray scattering study of the nucleation of GaN on sapphire(0001) by gas-source molecular-beam epitaxy. GaN growth using thermal ammonia and  $\text{Ga}(\text{C}_2\text{H}_5)_3$  exhibited a rapidly decaying intensity at the 0001 reflection, characteristic of three-dimensional cluster growth. Growth with 30-eV  $\text{NH}_x^+$  ions and  $\text{Ga}(\text{C}_2\text{H}_5)_3$  exhibited layer-by-layer intensity oscillations with maxima near odd-integer bilayers. The mode of nucleation is controlled by the Ga incorporation efficiency on the substrate and GaN islands. The Ga incorporation efficiency on the substrate is increased by a factor of 4 by low-energy ion irradiation during growth. [S0163-1829(98)09331-X]

### I. INTRODUCTION

Many solid-state devices depend on the formation of very perfect single-crystal thin-film layers. However, combining dissimilar materials by heteroepitaxy often results in the nucleation and growth of three-dimensional islands. This phenomenon is observed in many systems, such as GaAs/Si, GaP/Si, and SiC/Si.<sup>1,2</sup> The three-dimensional islands produce threading dislocations and planar defects as the islands coalesce.<sup>3,4</sup> These defects ultimately produce undesirable parasitic effects such as high threshold current in injection laser diodes. Consequently, a great deal of effort has been devoted to manipulating atomic-scale processes to produce smooth two-dimensional growth. Recently, GaN has attracted much attention because of its possible applications in blue light-emitting diodes, lasers, and other optoelectronic devices. However, the lack of GaN bulk crystals forces one to deposit GaN onto dissimilar substrates such as Si, SiC, or sapphire. The nucleation problem for GaN onto these materials is particularly severe because of a low incorporation efficiency of the metal-organic precursors typically used for growth.<sup>5</sup>

Several approaches have previously been developed for suppressing three-dimensional growth, including low-temperature buffer layers,<sup>6-8</sup> adsorbed foreign surface species (i.e., surfactants),<sup>9,10</sup> and low-energy ion-assisted growth.<sup>11</sup> Of these approaches, ion-assisted growth has received relatively little attention. However, for some materials systems ion- or plasma-assisted growth is the technique of choice. For example, GaN growth by molecular-beam epitaxy is usually performed using a plasma source<sup>12-15</sup> or a low-energy ion source<sup>16,17</sup> for nitrogen. At present, very little is known about the role of energetic precursors in the nucleation and growth of GaN other than the observation that plasma-assisted growth leads to the highest-quality films.<sup>13</sup>

In this article we discuss nucleation phenomena and subsequent growth of GaN on the (0001) surface of sapphire by gas-source (GS) molecular-beam epitaxy (MBE). Using

time-resolved x-ray scattering, we observe a profound change of growth mode when low-energy ions replace thermal ammonia molecules as the nitrogen source. Specifically, the specular reflectivity at the anti-Bragg position exhibits the classic layer-by-layer intensity oscillations associated with two-dimensional growth when  $\text{NH}_x^+$  ions are used and only a monotonic decrease in intensity (due to increasing roughness) when thermal ammonia is used. Layer-by-layer growth of the first few monolayers in a technologically relevant material system is particularly exciting, given that there are only a few examples of such phenomena in lattice-mismatched epitaxy.<sup>18-21</sup> The effect of ion-assisted growth is so dramatic that the technique effectively solves the GaN nucleation problem.

### II. EXPERIMENT

The experiments were performed on the A2 experimental station at the Cornell High Energy Synchrotron Source using radiation from a 1.2-T, 24-pole permanent magnet wiggler. X rays are directed onto a two-bounce  $\text{W/B}_4\text{C}$  synthetic multilayer monochromator with a 1% energy bandpass. The flux of monochromatic x rays at the sample is  $\sim 10^{12}$  photons per second in a 0.5 mm vertical by 1 mm horizontal beam spot at a wavelength of 0.1 nm. X rays impinge on the sample that is mounted inside an ultrahigh vacuum surface diffraction chamber with a base pressure of  $1 \times 10^{-10}$  Torr. The geometry is shown in Fig. 1. A detector arm with rotation stages for a crystal analyzer and a NaI(Tl) detector is mounted with both vertical and horizontal rotations about the sample surface. A graphite (0001) crystal analyzer with a mosaic width of  $0.4^\circ$  is used to filter out the fluorescent background. The resolution and the active area of the sample are defined by  $0.5 \times 1 \text{ mm}^2$  slits in front of the NaI(Tl) detector. A Si(Li) detector is mounted in the horizontal scattering plane to monitor the Ga  $K\alpha$  fluorescence, from which the deposition rate is determined.

The sapphire(0001) substrate is cleaned by degreasing

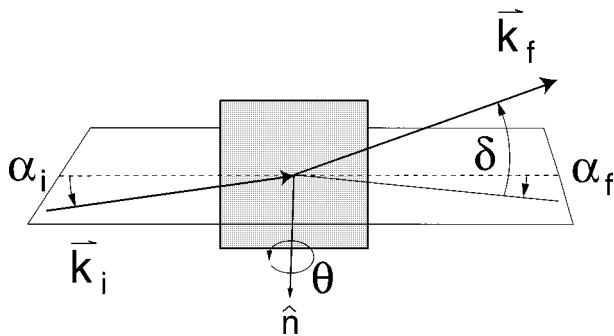


FIG. 1. Schematic diagram of the diffraction geometry. The GaN 0001 reflection is at  $\delta=0$  and  $\alpha_i=\alpha_f=5.6^\circ$ . Strain relaxation measurements are done with  $\alpha_i=\alpha_f\sim 0.3^\circ$  and scans of  $\delta$  from  $20^\circ$  to  $24^\circ$  with  $\theta=\delta/2$ .

and then etching in hot phosphoric acid.<sup>22</sup> After introduction into the vacuum chamber, the surface is cleaned in vacuum by heating to  $1000^\circ\text{C}$ . The temperature is determined by an infrared pyrometer. A nitridation layer is prepared by heating the sample to  $1000^\circ\text{C}$  with ammonia flowing at 50 SCCM (SCCM denotes cubic centimeter per minute at STP). The pressure under these conditions is  $\sim 1.5$  mTorr. Formation of a thin AlN layer is confirmed by monitoring the AlN  $[1\ 0\ \bar{1}\ 0.05]$  diffracted beam intensity. The thickness of the AlN layer reaches  $\sim 1.2$  nm after 10 min. For the case of thermal growth, the flux of trimethyl-gallium (TEG) and ammonia were  $9.6\times 10^{14}$  and  $2.8\times 10^{17}$   $\text{cm}^{-2}\text{s}^{-1}$ , respectively. The background pressure in the chamber under these conditions is  $3\times 10^{-4}$  Torr. For the ion-assisted case, a Commonwealth Mark-I End-Hall source is used to produce the 30-eV  $\text{NH}_x^+$  ions.<sup>23</sup> The ion-current density at the sample is  $3\times 10^{14}$   $\text{cm}^{-2}\text{s}^{-1}$ . All GaN films are deposited with excess ammonia, i.e., gallium-limited growth.<sup>24</sup> The crystallographic orientation of GaN and AlN relative to  $\text{Al}_2\text{O}_3$  is  $(0001)\parallel(0001)$  and  $[10\bar{1}0]\parallel[11\bar{2}0]$ .

### III. RESULTS

We first present results for film growth with real-time analysis in Sec. III A. The time dependence of the 0001 reflected intensity and the Ga  $K\alpha$  fluorescence intensity are monitored simultaneously during deposition and are typically recorded at a rate of one data point per second. Since x-ray absorption is negligible for the film thicknesses studied in these measurements, the intensity of the Ga  $K\alpha$  fluorescence x rays is directly proportional to the amount of Ga deposited on the surface. After the growth, Rutherford backscattering spectrometry (RBS) is used to calibrate the x-ray fluorescence intensity with film thickness and hence determine the growth rate. Contact mode atomic force microscopy (AFM) is used to image surface morphology. The AFM results are presented in Sec. III B. Measurements of strain relaxation during the growth process are described in Sec. III C. These measurements are performed using a modified real-time growth procedure: TEG flow is modulated in 2-s growth pulses with radial scans through the GaN and AlN  $[1\ 0\ \bar{1}\ 0.05]$  reflections between pulses.

#### A. Time-resolved measurements

Time-resolved x-ray measurements are performed to study the mode of nucleation by monitoring the surface mor-

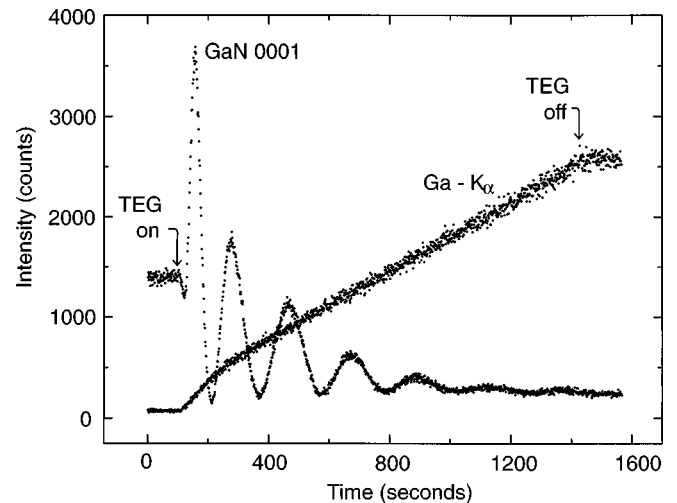


FIG. 2. Raw data as collected for ion-assisted growth of GaN on sapphire(0001) at  $600^\circ\text{C}$ . X-ray fluorescence intensity and reflected intensity at the GaN 0001 are plotted as a function of time. Growth is initiated and stopped when the TEG is turned on and off, respectively. X-ray fluorescence is used to monitor the amount of gallium deposited as a function of time, while reflectivity is a probe of surface morphology. The thickness of the film at the end of growth was 5.2 nm (20 bilayers).

phology and deposition rate as a function of film thickness. Figure 2 shows raw data as collected for ion-assisted growth of GaN on nitridated sapphire. The x-ray reflectivity at both the GaN 0001 and the Ga fluorescence signal are shown. A striking feature clearly present in the Ga  $K\alpha$  data is that the growth rate is higher for the first two bilayers and then decreases to a steady-state value. This effect is correlated with the growth mode, discussed below. Another remarkable feature is that the reflectivity signal exhibits intensity oscillations with a period that is inversely proportional to the growth rate. However, the peaks do not occur at exact integer monolayer thicknesses. The first peak is considerably more intense than the signal from the starting surface because of the higher electron density of GaN relative to sapphire. The peak intensity of the subsequent oscillations follows a decreasing envelope consistent with gradual roughening of the growth surface. As we will show below, the growth mode is induced by low-energy  $\text{NH}_x^+$  ion irradiation during growth.

Figure 3(a) is the same specular reflectivity data displayed in Fig. 2, plotted versus thickness instead of time. Maxima occur near odd bilayer thicknesses, but gradually fall out of phase with the mean thickness. Figure 3(b) is for identical growth conditions, except that the incident ammonia molecules have thermal energies ( $\sim 0.02$  eV). These conditions produce three-dimensional nucleation with a cluster separation of 35–50 nm and coalescence when the mean thickness is between 10 and 20 GaN bilayers.<sup>25</sup> The reflectivity data is *dramatically* different for this case, exhibiting a rapid decrease in intensity during the initial stages of nucleation and a slight recovery when island coalescence is complete. Figure 3(c) shows data for growth after preirradiation of the nitridated sapphire surface for 5 min. The growth conditions are identical to those in Fig. 3(b), except that the starting surface has been modified by ion irradiation. If we associate the maximum intensity with the coalescence of GaN islands, then the data suggest that island coalescence begins at ap-

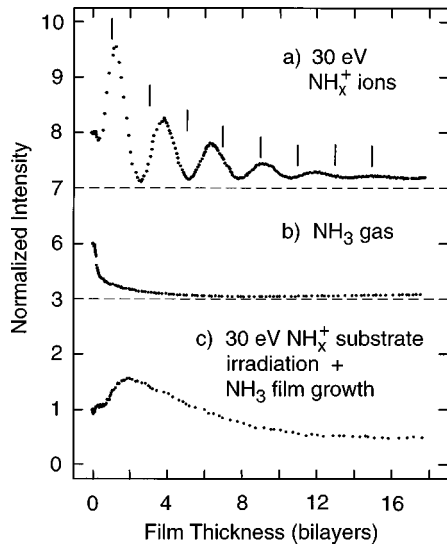


FIG. 3. Reflected intensity versus GaN deposited for three growth conditions: (a) growth with 30-eV  $\text{NH}_x^+$  ions and TEG (odd-bilayer thicknesses are indicated by tick marks above the data), (b) growth from ammonia and TEG, and (c) preirradiation with ions followed by growth from ammonia and TEG.

proximately two GaN bilayers, producing a single weak peak in the x-ray reflectivity data. This is followed by gradual roughening to a steady state. A comparison of Figs. 3(b) and 3(c) shows that the chemical and physical states of the starting surface influence the mode of nucleation. However, the quasi-layer-by-layer growth mode is observed only during reactive-ion-assisted growth as represented by Fig. 3(a).

Gallium incorporation efficiency depends on whether energetic ions are used. Figure 4 shows deposited gallium as a function of time. The data are from the same film growths as in Figs. 3(a) and 3(b). A large effect of ions on the growth rate is observed, both in the initial stages and during steady-state growth. The early-time behavior of growth without ions is dominated by low nucleation density, which results in a

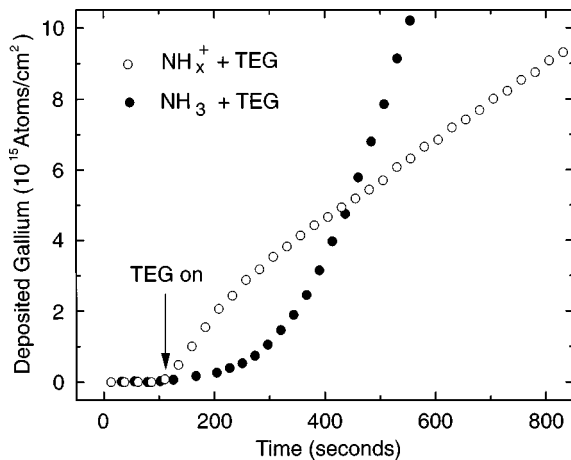


FIG. 4. Comparison of deposited GaN versus time for ion-assisted growth (open circles) and no ions (filled circles). The initial and final growth rates for ion-assisted growth are 0.020 and 0.012 bilayers/s, respectively. The initial and final growth rates for deposition from thermal ammonia are 0.005 and 0.067 bilayers/s, respectively. These values can be compared with a growth rate of  $\sim 1$  bilayer/s estimated for perfect incorporation of TEG.

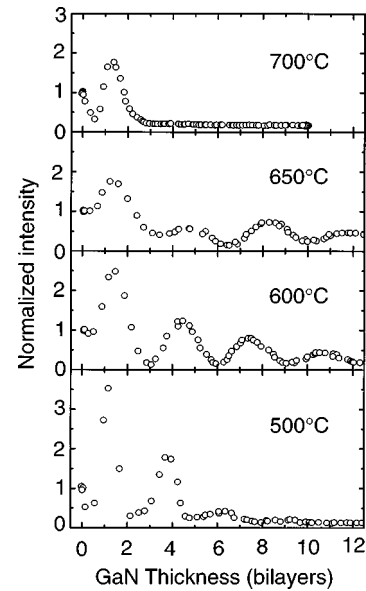


FIG. 5. Ion-assisted growth at four temperatures.

power-law growth rate of nuclei before coalescence.<sup>5</sup> Growth with ions results in an initial growth rate about four times higher. Curiously, the steady-state deposition rate for ion-assisted growth is reduced relative to conventional GS MBE. The low growth rate may be related to ion-enhanced desorption of TEG. Enhanced Ga desorption has been observed for GaN growth from elemental Ga and energetic  $\text{N}_2^+$  ions.<sup>16</sup> Passivation of the surface by hydrogen or excess surface nitrogen may also reduce the gallium incorporation efficiency.

The temperature dependence of the growth mode reveals several different features. Figure 5 shows 0001 reflectivity data at four temperatures. Growth at 500 °C exhibits classic layer-by-layer growth with gradual roughening due to limited surface mobility. The data for 600 °C and 650 °C follow a two-dimensional (2D) growth mode, but exhibit an unusual expansion of the period of the intensity maxima. It has been shown that this effect can arise from an asymmetry in the height distribution function of the surface.<sup>26</sup> In contrast, two-dimensional growth is observed at 700 °C for only the first 1–2 bilayers, followed by an abrupt drop in intensity. This is consistent with the Stranski-Krastanov growth mode, where a thin two-dimensional layer is followed by three-dimensional growth.

### B. Atomic force microscopy

Further insight into the surface morphology is obtained from AFM measurements performed after the completion of the growth. A postgrowth AFM analysis of the same samples has been performed. Figure 6 shows an AFM surface plot for the sample grown with ammonia as the nitrogen precursor at 600 °C. The rms surface width is 14.7 bilayers. The film thickness derived from RBS is 46 bilayers. The lateral separation of surface features is  $\sim 50$  nm. Figure 7 shows a surface plot for ion-assisted growth at 600 °C. The rms surface width is 3.6 bilayers and the film thickness derived from RBS is 20 bilayers. There is a clear difference in the surface morphology between ion-assisted growth and no-ion growth. Figure 8 shows a comparison of surface height probability

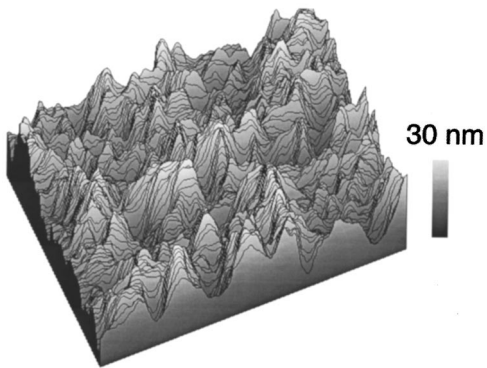


FIG. 6. AFM scan for GaN grown at 600 °C and ammonia as the nitrogen precursor. The vertical scale is 30 nm and the lateral scale is  $500 \times 500 \text{ nm}^2$ . The rms roughness of the surface is 14.7 GaN bilayers.

distributions for the two AFM images. The height profiles reveal another striking difference associated with ion-assisted growth. The profile for thermal ammonia growth has a nonzero value down to the sapphire/GaN interface, consistent with discrete cluster growth. In contrast, ion-assisted growth produces a continuous film with a much sharper height distribution. Another interesting feature is the asymmetry of the surface height distribution. The asymmetry can be characterized by an additional parameter that can be obtained from the surface height profiles, the third moment of the distribution. Following Bartelt and Evans,<sup>26</sup> we find a third moment  $\kappa_3$  of +0.27 and +1.25 for growth from thermal ammonia and ions, respectively. The sign of  $\kappa_3$  for the ion-assisted growth is consistent with the direction of the shift observed in reflectivity oscillations (Figs. 3 and 5). The sharp side of the distribution approximately defines the x-ray thickness, while the broad side represents isolated mounds ( $\kappa_3$  positive) or pits ( $\kappa_3$  negative).

The observed sign of  $\kappa_3$  is *opposite* to that from theoretical predictions for the model of molecular-beam epitaxy discussed by Bartelt and Evans.<sup>26</sup> In this model, upward currents (attributed to step-edge barriers faced by adatoms) break the up-down symmetry of the growth front. This leads to a negative value of  $\kappa_3$ . However, Amar and Family have shown that for the case of a large step barrier a positive skewness can be obtained.<sup>41</sup> Therefore, the positive skewness observed in our data may be consistent with a simple

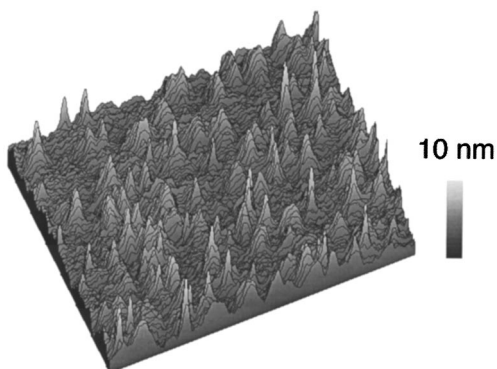


FIG. 7. AFM scan for GaN grown at 600 °C with ion-assisted growth. The vertical scale is 10 nm and the lateral scale is  $500 \times 500 \text{ nm}^2$ . The rms roughness of the surface is 3.6 bilayers.

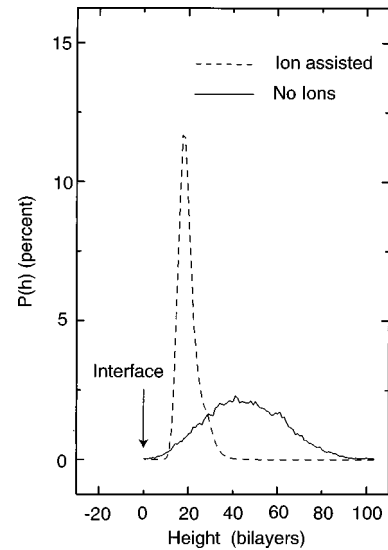


FIG. 8. Height probability distributions for the two AFM images. The distributions are aligned so that the GaN/sapphire interfaces are in registry for the two profiles and are indicated by an arrow.

model of epitaxial growth kinetics. However, strain-induced effects may also influence the growth morphology. We show below that the GaN films are significantly strained.

### C. Stepwise growth measurements

Due to the large lattice mismatch between sapphire and GaN, strain relaxation phenomena may be observed during the initial stages of growth. Figure 9 shows radial scans through AlN and GaN  $[1\ 0\ \bar{1}\ 0.05]$  positions as a function of

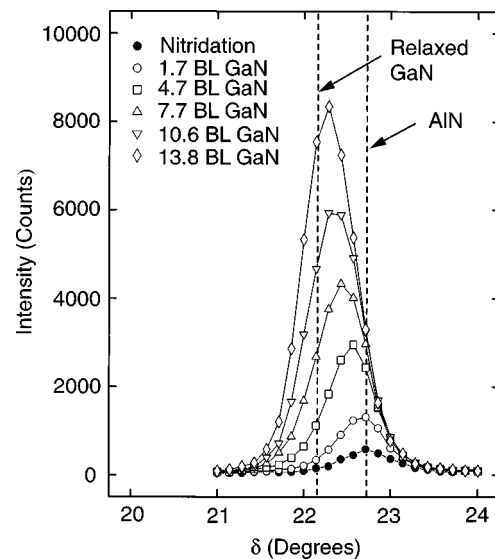


FIG. 9. Radial scans through the AlN and GaN  $[1\ 0\ \bar{1}\ 0.05]$  as a function of GaN thickness during ion-assisted growth. Data for GaN thicknesses of 0, 1.7, 4.7, 7.7, 10.6, and 13.8 bilayers are shown. The AlN layer is formed by nitridation of the  $\text{Al}_2\text{O}_3$  surface. Intensity increases as a function of GaN thickness, while the peak position gradually shifts. Calculated peak positions for AlN and relaxed GaN are shown for reference. The growth temperature is 600 °C.

GaN growth. The curve for the starting  $\text{Al}_2\text{O}_3/\text{AlN}$  structure formed by nitridation of  $\text{Al}_2\text{O}_3$  is aligned with the strain-relaxed AlN  $2\theta$  angle. Since the  $\sim 1.2$ -nm relaxed AlN layer has a relatively close lattice match to GaN, it is considered to be very favorable for the formation of high-quality GaN films.<sup>27</sup> The subsequent scans show that during GaN deposition at 600 °C, there is a *continuous* shift of the  $a$ -axis lattice parameter towards the relaxed position. Several other measurements of strain relaxation in the early stages of GaN growth have been reported in the literature. Kim *et al.* have found that GaN grown at 700 °C on an AlN buffer layer is coherently strained to the AlN in-plane lattice parameter up to a critical thickness of 11 bilayers.<sup>28</sup> In contrast, Daudin *et al.* have studied GaN growth at 720 °C on an AlN buffer layer and found a high degree of relaxation after four GaN bilayers.<sup>29</sup> They correlate strain relaxation with the formation of mounds in the early stages of growth. Our strain relaxation data for growth at 600 °C (Fig. 9) is intermediate between the two extremes, exhibiting partial relaxation before the critical thickness and almost complete relaxation above the critical thickness.

#### IV. DISCUSSION

The results above reveal a variety of phenomena that occur during the nucleation of GaN on nitridated sapphire. The real-time scattering and AFM results lead to a consistent picture of GaN nucleation and the effect of reactive ions during growth. It is immediately clear upon inspection of Figs. 2 and 4 that desorption effects play a dominant role in GaN nucleation and growth phenomena. We discuss desorption effects in terms of the incorporation coefficient, which can be defined as the probability of a Ga atom to be incorporated into the film for each TEG molecule impinging on the surface. The incorporation coefficient  $C$  varies locally, depending on the chemical and physical state of the surface. In particular, TEG molecules incident upon GaN islands have a different incorporation coefficient than TEG incident upon the AlN/sapphire substrate.<sup>5</sup> In Sec. IV A we discuss the case  $C_{\text{substrate}} \ll C_{\text{GaN}}$ , which leads to cluster nucleation. In Sec. IV B we discuss the case  $C_{\text{substrate}} \approx C_{\text{GaN}}$ , which leads to two-dimensional nucleation. In Sec. IV C we discuss the phenomenon of mound formation and its possible cause. In Sec. IV D we discuss the two-bilayer period observed in x-ray intensity oscillations.

##### A. Growth from thermal ammonia: Discrete cluster nucleation

The phenomena of three-dimensional cluster growth of GaN is related to incomplete incorporation of Ga onto the substrate.<sup>5</sup> This is reflected in Fig. 4 as an extremely small initial incorporation coefficient of about 0.005. We take this to be an upper limit for the value of  $C_{\text{substrate}}$ . A value of  $C_{\text{GaN}} = 0.067$  is obtained from the final growth rate after coalescence of nuclei. Thus the ratio of coefficients is  $\sim 13$ . This growth configuration leads to a low density of *discrete* clusters. The mechanism is the same for GaN growth on several substrates, including Si, SiC, and sapphire.<sup>5</sup>

Because of the very small value of  $C_{\text{substrate}}$ , incorporation of Ga is determined by the rate of direct impingement of Ga atoms onto existing GaN nuclei. The rate of Ga incorporation is therefore approximately proportional to their surface

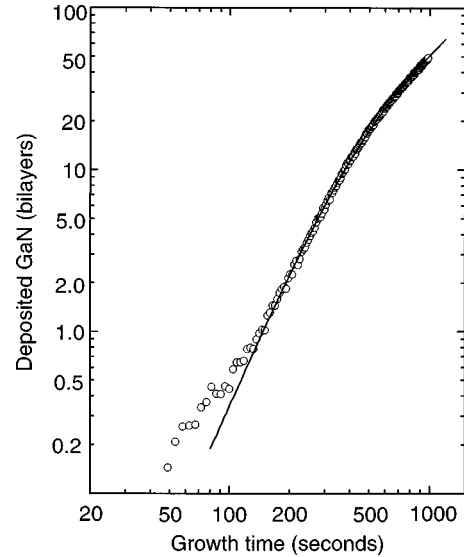


FIG. 10. Fit to Ga fluorescence data using the three-dimensional cluster growth model. The crossover from cluster nucleation to coalescence is clearly visible in the data.

area. Additional nucleation can be neglected compared to the rate of growth of nuclei, except in the very early stage when the size of nuclei is very small. This phenomenon leads to approximately a power-law function of time in the fluorescence data. This model can be confirmed by plotting the fluorescence data on a log-log plot, as shown in Fig. 10. An empirical expression for the growth rate including both the power-law growth and the linear regime after coalescence is

$$R(t_r) \approx R_\infty (1 - e^{-t_r^{\nu-1}}), \quad (1)$$

where the reduced time  $t_r$  is equal to  $t/t_\times$  and the crossover from nucleation to coalescence is given by  $t_\times$ . The steady-state growth rate is  $R_\infty$  and the growth exponent is  $\nu$ . This expression gives the desired limits since  $R \sim t^{\nu-1}$  and the total amount of incorporated Ga  $\theta \sim t^\nu$  when  $t_r \ll 1$ . Also,  $R = R_\infty$  when  $t_r \gg 1$ . The solid line in Fig. 10 is for a numerical integration of Eq. (1) with  $\nu = 2.85$  and  $R_\infty = 0.067$ . The curve gives a reasonable description of the crossover from cluster growth to coalescence of clusters. However, for  $t < 100$  s, another mechanism (such as nucleation or surface-diffusion limited growth of nuclei) dominates the uptake curve.

##### B. Growth from low-energy ions: Two-dimensional nucleation

In the preceding subsection we described how low incorporation on the substrate leads to discrete cluster growth. Figure 4 shows that this situation is reversed for ion-assisted growth, i.e., incorporation is higher for the first several layers, than during subsequent growth. From the data we estimate  $C_{\text{GaN}} = 0.012$ ,  $C_{\text{substrate}} = 0.020$ , and a ratio of  $\sim 0.6$ .

Tersoff *et al.*<sup>30</sup> introduced the following model that can be used to explain a transition from two- to three-dimensional growth. The nucleation density on the starting surface produces a mean separation between nuclei  $L_n$ . When their radius becomes larger than a critical value  $R_C$ , a second layer will nucleate. If  $R_C \ll L_n$ , the process is repeated for the second, third, and subsequent layers, resulting in multilayer islands. However, if  $R_C > L_n$ , then the islands

will coalesce before the second layer can nucleate, producing two-dimensional growth. This model is consistent with our data since the enhanced value of  $C_{\text{substrate}}$  that we observe during ion-assisted growth should lead to a large reduction in  $L_n$  and to 2D growth. Figure 3(a) is therefore interpreted as a high nucleation density, while Fig. 3(b) is associated with a low nucleation density.

There are several mechanisms that would lead to reactive-ion irradiation producing enhanced incorporation of Ga. Enhanced reactivity of  $\text{NH}_x^+$  or  $\text{N}^+$  relative to ammonia is the effect generally cited in the literature for the success of plasma-assisted growth of GaN. However, Fig. 4 shows that ion-assisted growth does not necessarily result in a higher steady-state growth rate, as is often assumed. Several purely physical mechanisms have been discovered that promote two-dimensional growth. For example, ion-induced layer-by-layer growth was reported for the Cu/Cu(111) system induced by pulsed beams of 500-eV argon ions.<sup>31</sup> The results were attributed to increased two-dimensional island density from ion bombardment.<sup>31</sup> It has also been proposed that energetic ions can break up three-dimensional islands.<sup>11</sup> Creation of surface defects such as vacancies or adatoms by energetic ions can also lead to an enhanced nucleation density since surface defects may act as nucleation sites. Figure 5(c) suggests that surface defect sites such as steps, kinks, vacancies, or other defects can dramatically alter the nucleation kinetics. Therefore, a limited amount of surface damage using ion energies below the bulk displacement threshold may actually be beneficial for producing planar growth.

### C. Surface height profile asymmetry

A pronounced asymmetry in the surface height profile is observed in AFM images. Figures 7 and 8 show that this effect is related to the formation of well-separated mounds on an otherwise flat growth surface. We have performed additional AFM measurements and find rms roughnesses of 4.0, 3.6, 1.2, and 7.1 bilayers for 500 °C, 600 °C, 650 °C, and 700 °C, respectively. The large rms value for 700 °C suggests a breakdown of 2D growth, in agreement with the x-ray data in Fig. 5. The values of the third moments also show a trend. From low temperature to high temperature, the values of  $\kappa_3$  are 1.63, 1.25, 2.20, and 3.14. This trend is consistent with the increasing shift of the 0001 x-ray reflectivity intensity maxima with increasing temperature observed in Fig. 5.

The temperature dependence of the roughness and surface asymmetry suggests the following model of the surface evolution. Low-temperature growth produces random roughness because of low surface mobility and statistical noise in the arrival rate on different parts of the surface. Therefore, surface diffusion plays a role in determining surface morphology. This explains the initial decrease of roughness with increasing temperature. At higher temperatures, smoothing by surface diffusion is countered by a mechanism that favors mound formation, such as a large step-edge barrier.<sup>41</sup> This leads to an instability of the surface morphology that is most pronounced at the highest growth temperatures. The combination of these two effects leads to the observed behavior where the rms surface roughness first decreases and then increases as a function of temperature. This model for the formation of roughness may explain the unusual cusplike

structures observed in Fig. 7. We associate the formation of cusplike mounds with the increasing third moment as a function of growth temperature.<sup>16,32</sup>

The mounds are also reminiscent of self-assembled structures formed in  $\text{In}_y\text{Ga}_{1-y}\text{As}$  on GaAs and  $\text{Ge}_y\text{Si}_{1-y}$  on Si thin-film systems.<sup>33–36</sup> In these systems, strain-driven mounds are not stable if they are smaller than a critical size since there is a competition between elastic energy and surface tension. In an equilibrium theory, once mounds reach a critical size they grow rapidly by a ripening process.<sup>37</sup> In the case of GaN growth, the temperature-dependent x-ray reflectivity and AFM data are consistent with mound formation by a strain-driven surface instability. However, we have not observed any changes in morphology during annealing up to 800 °C. This suggests that mounds are kinetically constrained from reaching an equilibrium configuration.

### D. Intensity oscillations during heteroepitaxy: The two-bilayer period

The familiar case of layer-by-layer growth is for homoepitaxy where intensity oscillations have a period of one monolayer.<sup>38–40</sup> In contrast, we observe intensity maxima only near *odd-integer* values. This phenomenon is related to the diffraction structure factor resulting from the growth of a relatively high-electron-density film on a low-electron-density substrate. At the GaN 0001 reflection, the film contribution to the scattering amplitude at even-bilayer thicknesses is exactly zero, neglecting the effects of surface roughness. Therefore, the intensity at even-integer thickness is related to the scattering amplitude of the substrate. This simple analysis suggests that there should be smaller, but observable, intensity maxima at even-integer values. However, a more realistic model including roughening of the GaN growth front shows that the even maxima are much more sensitive to roughness than the odd maxima. We conclude that the intensity oscillation data are consistent with a growth process in which only one bilayer at a time forms in a layer-by-layer growth mode. Finally, intensity maxima do not necessarily coincide with integer monolayer thicknesses if the surface height distribution is asymmetric.

## V. CONCLUSIONS

In summary, we have experimentally discovered a dramatic effect of low-energy ions on the nucleation kinetics of GaN on sapphire. Film growth rates approximately follow a power law during nucleation by gas-source MBE. In contrast, ion-assisted growth produces a dramatic increase of the incorporation efficiency of Ga at the start of deposition and hence provides a method for controlling the nucleation and growth mode. The temperature dependence of x-ray intensity oscillation data is consistent with limited mound formation resulting from a surface instability related to growth kinetics.

## ACKNOWLEDGMENTS

We thank David Goodstein and Barbara Cooper for helpful discussions. This work was supported by the National Science Foundation under Grant Nos. DMR-9311772 (Cornell High Energy Synchrotron Source) and DMR-9632275 (Cornell Materials Science Center).

- <sup>1</sup>J. E. Palmer, G. Burns, G. C. Fonstad, and C. V. Thompson, *Appl. Phys. Lett.* **55**, 990 (1989).
- <sup>2</sup>F. Ernst and P. Pirouz, *J. Mater. Res.* **4**, 834 (1989).
- <sup>3</sup>H. L. Tsai and R. J. Matyi, *Appl. Phys. Lett.* **55**, 265 (1989).
- <sup>4</sup>E. A. Fitzgerald, *JOM* **41**, 20 (1989).
- <sup>5</sup>R. L. Headrick, S. Kycia, Y. K. Park, A. R. Woll, and J. D. Brock, *Phys. Rev. B* **54**, 14 686 (1996).
- <sup>6</sup>D. S. Wu, R. H. Horng, and M. K. Lee, *Appl. Phys. Lett.* **54**, 2244 (1989).
- <sup>7</sup>S. M. Koch, S. J. Rosner, R. Hull, G. W. Yoiffe, and J. S. Harris, Jr., *J. Cryst. Growth* **81**, 67 (1987).
- <sup>8</sup>R. M. Lum, J. K. Klingert, B. A. Davidson, and M. G. Lamont, *Appl. Phys. Lett.* **51**, 36 (1987).
- <sup>9</sup>M. Copel, M. C. Reuter, E. Kaxiras, and R. M. Tromp, *Phys. Rev. Lett.* **63**, 632 (1989); M. Copel, M. C. Reuter, M. Horn von Hoegen, and R. M. Tromp, *Phys. Rev. B* **42**, 11 682 (1990); F. K. LeGoues, M. Copel, and R. M. Tromp, *ibid.* **42**, 11 690 (1990).
- <sup>10</sup>H. A. van der Vegt, H. M. van Pinxteren, M. Lohmeier, E. Vlieg, and J. M. C. Thornton, *Phys. Rev. Lett.* **68**, 3335 (1992).
- <sup>11</sup>C.-H. Choi and S. A. Barnett, *Appl. Phys. Lett.* **55**, 2319 (1989); C.-H. Choi, L. Hultman, R. Ai, and S. A. Barnett, *ibid.* **57**, 2931 (1990); C.-H. Choi, R. Ai, and S. A. Barnett, *Phys. Rev. Lett.* **67**, 2826 (1991); J. Mirecki Millunchick and S. A. Barnett, *Appl. Phys. Lett.* **65**, 1136 (1994).
- <sup>12</sup>R. F. Davis, Z. Sitar, B. E. Williams, H. S. Kong, H. J. Kim, J. W. Palmour, J. A. Edmond, J. Ryu, J. T. Glass, and C. H. Carter, *Mater. Sci. Eng., B* **1**, 77 (1988).
- <sup>13</sup>M. A. L. Johnson, Shizuo Fujita, W. H. Rowland, Jr., K. A. Bowers, W. C. Hughes, Y. W. He, N. A. El-Masry, J. W. Cook, Jr., J. F. Schetzina, J. Ren, and J. A. Edmond, *J. Vac. Sci. Technol. B* **14**, 2349 (1996).
- <sup>14</sup>S. Strite and H. Morcoç, *J. Vac. Sci. Technol. B* **10**, 1237 (1992); S. Strite, M. E. Lin, and H. Morcoç, *Thin Solid Films* **231**, 197 (1993).
- <sup>15</sup>M. J. Paisley, Z. Sitar, J. B. Posthill, and R. F. Davis, *J. Vac. Sci. Technol. A* **7**, 701 (1989).
- <sup>16</sup>R. C. Powell, N.-E. Lee, Y.-W. Kim, and J. E. Greene, *J. Appl. Phys.* **73**, 189 (1993).
- <sup>17</sup>M. Rubin, N. Newman, J. S. Chan, T. C. Fu, and J. T. Ross, *Appl. Phys. Lett.* **64**, 64 (1994).
- <sup>18</sup>Weak reflection high-energy electron diffraction intensity oscillations have been observed during  $\text{In}_y\text{Ga}_{1-y}\text{As}$  growth on GaAs; C. W. Snyder, B. G. Orr, D. Kessler, and L. M. Sander, *Phys. Rev. Lett.* **66**, 3032 (1991).
- <sup>19</sup>An interesting example of layer-by-layer oscillations in a lattice-mismatched system occurs for the first 2–3 ML of organic thin film epitaxy on a Au(111) substrate; P. Fenter, P. Eisenberger, P. Burrows, S. R. Forrest, and K. S. Liang, *Physica B* **221**, 145 (1996).
- <sup>20</sup>Intensity oscillations in electron diffraction patterns from the first three monolayers of CdSe grown on ZnSe have been observed; S. Fujita, Y.-H. Wu, Y. Kawakami, and S. Fujita, *J. Appl. Phys.* **72**, 5233 (1992).
- <sup>21</sup>Intensity oscillations have been observed in reflection high-energy electron diffraction for heteroepitaxial metal systems, including Fe on Cu(100) and Cu, Fe, and Mn on Ag(100); W. F. Egelhoff, Jr. and I. Jacob, *Phys. Rev. Lett.* **62**, 921 (1989).
- <sup>22</sup>A 400-nm-thick layer of molybdenum is sputter deposited on the back of the sapphire substrate to improve the efficiency of the radiant heater.
- <sup>23</sup>Commonwealth Scientific Incorporated, Alexandria, VA.
- <sup>24</sup>R. Held, D. E. Crawford, A. M. Johnston, A. M. Dabiran, and P. I. Cohen, *J. Electron. Mater.* **26**, 272 (1997).
- <sup>25</sup>R. L. Headrick *et al.* (unpublished).
- <sup>26</sup>M. C. Bartelt and J. W. Evans, *Phys. Rev. Lett.* **75**, 4250 (1995).
- <sup>27</sup>N. Grandjean, J. Massies, and M. Leroux, *Appl. Phys. Lett.* **70**, 643 (1997).
- <sup>28</sup>C. Kim, I. K. Robinson, J. Myoung, K. Shim, M.-C. Yoo, and K. Kim, *Appl. Phys. Lett.* **69**, 2358 (1996).
- <sup>29</sup>B. Daudin, F. Widmann, G. Feuillet, Y. Samson, M. Arlery, and J. L. Rouvière, *Phys. Rev. B* **56**, R7069 (1997).
- <sup>30</sup>J. Tersoff, A. W. Denier van der Gon, and R. M. Tromp, *Phys. Rev. Lett.* **72**, 266 (1994).
- <sup>31</sup>G. Rosenfeld, N. N. Lipkin, W. Wulfhekel, J. Kliewer, K. Morgenstern, B. Poelsema, and G. Comsa, *Appl. Phys. A: Mater. Sci. Process.* **61A**, 455 (1995).
- <sup>32</sup>F. A. Ponce, J. J. S. Major, W. E. Plano, and D. F. Welch, *Appl. Phys. Lett.* **65**, 2302 (1994).
- <sup>33</sup>S. Guha, A. Madhukar, and K. C. Rajkumar, *Appl. Phys. Lett.* **57**, 2110 (1990).
- <sup>34</sup>F. Houzay, C. Guille, J. M. Moison, P. Henoc, and F. Barthe, *J. Cryst. Growth* **81**, 67 (1987).
- <sup>35</sup>Y.-W. Mo, D. E. Savage, B. S. Swartzentruber, and M. G. Lagally, *Phys. Rev. Lett.* **65**, 1020 (1990).
- <sup>36</sup>D. J. Eaglesham and M. Cerullo, *Phys. Rev. Lett.* **64**, 1943 (1990).
- <sup>37</sup>I. Daruka and A.-L. Baribási, *Phys. Rev. Lett.* **79**, 3708 (1997).
- <sup>38</sup>C. E. C. Wood, *Surf. Sci. Lett.* **108**, L441 (1981).
- <sup>39</sup>C. J. H. Neave, B. A. Joyce, P. J. Dobson, and N. Norton, *Appl. Phys. A: Solids Surf.* **A31**, 1 (1983).
- <sup>40</sup>J. M. Van Hove, C. S. Lent, P. R. Pukite, and P. I. Cohen, *J. Vac. Sci. Technol. B* **1**, 741 (1983).
- <sup>41</sup>J. G. Amar and F. Family, *Phys. Rev. B* **54**, 14 742 (1996).